# Direct Imaging of Atomic-Scale Ripples in Few-Layer Graphene

# Direct imaging of atomic-scale ripples in few-layer graphene

Wei L. Wang[1,2], Sagar Bhandari[2], Wei Yi[2†], David C. Bell[3], Robert Westervelt[1,2], Efthimios Kaxiras[1,2⋆]

[1] *Department of Physics, Harvard University, Cambridge, Massachusetts 02138, USA*

[2] *School of Engineering and Applied Sciences, Harvard University, Cambridge, Massachusetts 02138, USA*

[3] *Center of Nanoscale Systems, Harvard University*

† *Current Address: HP Labs Palo Alto, USA*

⋆*e-mail: kaxiras@physics.harvard.edu*

**Ultra-thin materials, ranging from bio-membranes to graphene [1, 2], are featured with extreme structures and important functional properties. In the thinnest limit, graphene demonstrates that a free-standing single atomic layer could be stable and strong [3, 4]. However, both theory [5, 6] and experiments [3, 7] suggest that graphene exists only because of intrinsic ripples that suppress the long-wavelength thermal fluctuations which would otherwise crumple the membrane. In experiment, the evidence of the ripples in graphene has been observed as smeared diffraction spots in reciprocal space [3, 7]. Imaging the ripples in real space and obtaining spatial information has been illusive because the small height variation is hard to detect locally. In this letter, we show direct real-space images of the ripples in a few-layer graphene (FLG) membrane resolved at the atomic-scale using monochromatic aberration-corrected transmission electron microscopy (TEM). In a FLG, the local effects of the ripples are amplified by the thickness, resulting in spatially-varying TEM contrast that is unique up to inversion symmetry. We compare the characteristic patterns observed in TEM with simulated images based on an accurate first-principles total potential. Our results shed lights on the ripples in real space, and suggest that the presence of intrinsic ripples is likely common for ultra-thin materials even in the nanometer-thickness range.**

The significance of the discovery of graphene [2] lies not only in its potential as a novel material for electronics [1], but more fundamentally, in demonstrating that the ultimate limit of thinness in a material membrane is attainable. Prior to the realization of this single-atomic layer of carbon membrane, the thinnest material ever freely suspended over a gap was in a range of tens of atomic layers, for example, a 15 nm nanocrystaline silicon film [8]. Theory predicted that in the limit of the ultimately-thin material, a two dimensional (2D) system cannot survive at finite temperature because thermal fluctuations would spontaneously destroy the long range order of a 2D crystal [9]. Meyer *et al.* [3] showed that a free-standing single atomic layer of graphene does exist, but in a nearly 2D form that has random elastic deformation in the third dimension [3, 7], as is indicated by the smeared spots in electron diffraction patterns. The smearing was attributed to atomic-scale ripples that has been described in a previous theory [5, 10] as the result of decoupling of the bending and stretching long-wavelength phonon modes [6]. The ripples appear to be an intrinsic

property of thin membranes that affect their mechanical, electric and magnetic properties [11–16]. Despite these advances in understandings materials at the limit of thinness, there are still many open issues. One of essential importance is what exactly the ripples look like in real space and whether or not they exist for strictly 2D systems.

Observation of the ripples is not straightforward because it requires both imaging at the atomic scale and detection of small deviations from flatness. Electron diffraction [3, 19] is sensitive but cannot capture spatial information, while convergent beam electron diffraction (CBED) [19] is limited by spatial resolution and image interpretation. Although bond length variations in a high resolution TEM image [17] can be related to the local tilt resulting from ripples, the detection sensitivity is rather low, corresponding to only a couple of pixels per bond for typical ripples. It is possible to observe the ripples in thicker samples [3] but only if the thickness does not suppress the ripples altogether. In this letter, we show atomically resolved images of a free standing few-layer graphene (FLG) membrane that exhibits aperiodic spatially-varying patterns. In FLG samples, a small deviation of the normal results in an amplified change in the projected potential, which shifts the phase of passing electron waves and leads to changes in the image contrast. These local contrast patterns serve as fingerprints of the local tilt of the column of the carbon atoms in the rippled crystalline thin film. We show through TEM image simulations that by varying the surface normal systematically, we are able to produce images that match the observed patterns and the obtained gradient field can be used to determine the topography of the ripples.

In simulating the TEM images and mapping to the experimental data, it is important to reproduce accurately the projected total potential felt by the electrons as they pass through the specimen, which determines the image patterns. The total potential includes both single-particle terms and exchange-correlation effects. TEM images are routinely simulated using an approximation called independent atomic model (IAM) [18]. This model superimposes single atomic potentials in the system and neglects all bonding effects, including the redistribution of electronic charge and the corresponding changes in the total potential. IAM is adequate in many cases for qualitative image interpretation, particularly in conventional TEM where substantial aberration is present that smears out the detailed effects due to bonding. With the recent development of aberration correction in electron optics of TEM, imaging resolution has been improved significantly and IAM has been found inadequate in

detailed quantitative and even qualitative analysis [19]. To account for bonding effects on the total potential, realistic first-principles methods based on, for example, density functional theory (DFT) must be used. Most efficient DFT codes utilize pseudopotentials and therefore yield the wrong total potential in the core region. To remedy this issue, all-electron codes can be used [19], but as the system size increases, the computational cost for all-electron calculations becomes prohibitive because of nearly exponential scaling. Here we develop a straightforward procedure to efficiently obtain the realistic total potential including bonding effects, using pseudopotentials within DFT, and then correct the core region potential with a term extracted from all-electron calculations of single atoms.

The graphene samples are mechanically exfoliated from natural graphene flakes using the standard scotch tape method [2]. The samples of interest are subsequently floated on water and deposited on standard TEM grids using a hydrophobic film [20]. The advantages of this method are that the area of interest in the sample can be aligned precisely on the open windows of the TEM grid, and that the contaminations from the scotch tape and the preparation processes are minimized. Raman spectra [21] (Fig. 1a) taken before and after the transfer process show identical signatures in the identified single-layer and multiple-layer areas, excluding the possibility of mechanical damage or substantial contamination during the process.

We image the TEM samples with Libra 200 MC by Zeiss, a monochromatic aberration corrected TEM operated at 80 kV. The combination of objective-lens Cs correction and a FEG-source monochromator considerably improves the spatial and energy resolutions [22]. The electron beam from the field emission gun is energy filtered and passes through a selected 3.5 $\mu$m slit, which limits the energy spread of the beam to $\Delta E < 0.1$ eV. The reduced spread of the beam energy expands the temporal coherence envelope function and increases the information limit. Fig. 1c shows an image of a FLG, where the fast Fourier transform (inset) indicates that the resolution is better than 0.79 Å, (which is well below the carbon-carbon bond length 1.42 Å), yielding not only a clearly resolved graphene lattice but also the fine contrast details beyond the graphene lattice frequency. It is important here for us to push the information limit to the higher frequencies than that is required to resolve graphene lattice because the variation of the fine details in the TEM contrast would otherwise not be observed. Fig. 1b shows the image of the edge of a selected FLG area. The fold at the edge reveals that the membrane has 11 layers. At a nominal magnification of $10^6$,

the image is of high quality across the entire scope, an area of 50 nm $\times$ 50 nm. Slight low frequency strips could be present in the image after exposure for extended time, which is attributed to the charge of the energy limiting slit. The strips can be readily filtered out if necessary, but since they are low in amplitude and well decoupled from the relevant graphene lattice frequency, they do not affect the subsequent analysis. The observed lattice in the TEM image is consistent with the known lattice constant of graphene. What is puzzling in the image is that the contrast exhibits significantly varying patterns that gradually evolve spatially, as is highlighted in Fig. 1e. In Fig. 1d, superimposed on the original full scope image, we show TEM contrast patterns at a $4\times3$ array of sampled locations. At each sampled location, we magnify the unfiltered image and show the local TEM contrast pattern that is enlarged 8 times. The pattern is distinctly different from Moiré fringes or periodic buckling patterns observed in samples with lattice mismatch, typical in chemically processed FLG [23, 24]. Those samples all exhibit in their TEM image periodicity larger than the primary cell of graphene, which originates from lattice mismatch and beating. Our FLG samples are minimally processed and free of interactions with harsh chemicals. The patterns we observe have exclusively the periodicity that corresponds to the primary cell of graphene, but vary in appearance with location. This can only be explained by location-dependent slight tilt of the sample normal, that is, static rippling of the graphene membrane. The local tilt of the membrane modifies the projected potential of the carbon atom columns in the crystal, which in turn changes the TEM image contrast. This interpretation is also supported by the observed dynamic range variation in the TEM contrast, which gradually decreasing from the left side to the right in Fig. 1e. The dynamic range reduction is a result of increased deviation of the local normal from the TEM optical axis which makes the projected potential more uniform and therefore reduces the image contrast.

To further understand these patterns and quantify the observations, it is necessary to conduct TEM image simulations and compare with the experimental data. The image simulation starts with the specimen potential. We have developed a general strategy to calculate the accurate total potential of bonded systems in both core and bonding regions by applying a transferable core correction. In preparing the core-correction potential, we first obtain potentials for a carbon atom using DFT based on both all-electron and pseudopotential calculations. We then subtract the pseudopotential part from the all-electron potential. The resultant core potential correction $V_{cc}$, shown in Fig 2. has a short cutoff at 0.6 Å.

Assuming the core potential is largely unaffected during bonding, this core correction is generally transferable and can be applied to the total potential $V_{ps}$ obtained by the efficient calculations based on pseudopotentials. In bonded systems, the total potential $V_{ps-cc}$ based on pseudopotential DFT with the core correction (psDFT-cc) reproduces well the correct potential in both core and bonding regions. On the other hand, it is clear that the IAM potential $V_{IAM}$, is substantially different in amplitude. This is expected because for an independent atom the potential is screened over a long distance while in the bonded system the screening of the core potential is much more effective. The difference contributes not only to an underestimated background, but also to different contrast in the projected potential, as is shown in the inset of Fig. 2a. The error may not make a noticeable difference in traditional TEM where substantial spherical aberration is present. However, for a quantitative analysis based on aberration corrected images, the error may lead to quantitatively or even qualitatively wrong results [19]. In our imaging of the ripples in FLG, we manage to minimize the beam energy spread and spherical aberration to achive imformation transfer beyond the graphene lattice frequency so that fine-detailed TEM contrast images can be obtained. Fig. 2b shows that as the information transfer improves, the higher frequencies components in the potential difference between DFT and IAM are transferred more effectively, resulting in larger difference in the final TEM images. Therefore it is essential to use accurate first-principles potential in our simulations and interpretations of the high-resolution images of the rippled FLG system.

Once the total potential of the FLG system is obtained, it is projected along the given local tilt directions, and used in the subsequent TEM image simulations. Indeed, by systematically varying the tilt angle, experimentally observed atomic-scale pattern variations are readily reproduced. Fig. 3a shows, for various patterns, the comparison between the experimental unfiltered TEM images and the matched images from the simulations. We compute an array of simulated TEM images using discreet values of inclination angles $\theta_x$ and $\theta_y$, varying between $-7^o$ and $+7^o$ with an increment of $0.5^o$. From the experimental TEM image, we selected a $20 \times 20$ array of local images, which is then compared to each of the simulated images. The normalized cross-correlation is computed for each comparison to identify the best possible matching index $C$ (as defined in Methods) which is typically better than 90%. The exhaustive search allows matching each local TEM contrast pattern to inclination angles with a resolution of $\pm 0.5^o$. The simulated images can effectively match

the various patterns from the experiment only by including relatively large inclination angle up to $\pm 7^o$. It is important to check if the mapping from the TEM image contrast pattern to the inclination angles is unique so that the value of inclination at each point is determined without ambiguity. For a column of atoms, the projected potential is solely dependent on the inclination angle. Two different inclination angles lead to potential projections that are different in anisotropy and density distribution, unless the inclination angles are of the same amplitude and opposite in sign. Because of the $C_2$ symmetry of the projected potential, as shown in the example of Fig. 3c the best matching is only determined up to inversion symmetry with respect to the inclination angle. Additional imaging restrictions can be imposed to eliminate the inversion symmetry ambiguity. As observed in the experimental image, the pattern changes gradually with location (Fig. 1f) which indicates that the surface is smooth and the change of inclination angle is continuous. This is physically reasonable since an abrupt change of inclination angle implies a structural discontinuity, which is typically accompanied by a large energy cost. By imposing the continuity condition in the gradient of the surface, the inclination angle can be uniquely found once the nearby gradient is known. This property allows us to determine the entire surface gradient map, up to global inversion symmetry.

The gradient field obtained from matching experimental data to simulation results can then be used to reconstruct the topography of the graphene membrane. We utilize a Fourier transform based nonlocal algorithm that is accurate for smooth surfaces with integrable gradient field [25]. Fig. 4a shows the reconstructed topography of the graphene membrane. In Fig. 4b, the gradient fields in the x and y directions are compared to the gradient fields calculated from the reconstructed surface. The standard deviation is 0.01, reasonably consistent with the resolution of the matched inclination angles that are determined at each sampling point. The integrability of the matched gradient field is a verification that the matching is accurate within the given resolution of $\pm 0.5^o$. In the contour plot, we identify a characteristic wavelength of 30 nm and a maximum deviation of 0.5 nm for the given area of $50 \times 50$ nm, which is in agreement with previous experimental analysis [3, 17]. Specifically, on single layer graphene using electron diffraction, where the spatial information is not directly available, the amplitude is estimated to be 1 nm based on the coherence length, the illuminated area size, and the local normal tilt angles [3]. Previous simulations [6] on single layer graphene give a wavelength $\sim 8$ nm at 300K, four times smaller than in our sample

which is ten times thicker. This is consistent with the trend that, for a thicker membrane with larger bending momentum, one expects the anharmonic coupling to take effect at a larger wavelength, thereby shifting the peak in the correlation function of the normals to lower frequencies. The same simulation [6] yielded a ripple amplitude of 0.7 Åat 300K, which is an order of magnitude smaller than what is reported in most experiments. According to the predictions of the phenomenological model on flexible membranes, the mean-square displacement in the direction normal to the layer is $< h^2 > \propto TL^2/\kappa$ where $L$ is the linear size of the sample and $\kappa$ is the bending rigidity. The temperature $T$ here is not precisely known. In our high resolution TEM imaging, high brightness is required and the electron beam flux in the illuminated area on the ample is high, on the order of 1 pA/nm$^2$. It is possible that electron irradiation raises the temperature in the imaged area and contributes to the larger amplitude of ripples, compared to the value at room temperature conditions or in the TEM diffraction mode. Our observation also confirms that the ripples are static, at least on the 10 second time scale that the image is taken. Otherwise, the spatially-varying fingerprints of the ripples we observed would have been smeared or averaged out.

Our direct real-space observation and analysis of the TEM characteristic patterns contributes to the understanding of the atomic-scale ripples, a fundamentally new phenomenon that is likely common for ultra-thin materials in the 2D and nearly-2D range. Even when supported on a substrate, the ripples are not entirely suppressed and are bound to affect the properties of the ultra-thin material considerably [11–16]. Besides graphene, a family of single atomic layer materials such as BN, $MoS_2$, $Bi_2Sr_2CaCu_2O_x$, have been identified in experiment[26], although it is not yet clear if all would survive suspension, since bonding topology and strength might affect the stabilization mechanism of the ripples. From single atomic layer to few layers and to the nanometer thickness range there are numerous possibilities of forming layered and non-layered ultra-thin systems of novel composition. It would be interesting to observe the possible presence of the intrinsic ripples in such systems and see how the ripples play a role in their structural stability and functional properties.

## METHODS

**Preparation of suspended graphene membrane sample for TEM imaging.** The graphene sample is obtained from natural graphite flakes (Asbury Carbons Co.) that are subjected to repeated mechanical exfoliation with low contamination SEC blue tape (Loomis Industries) and pressed on a silicon wafer with

285 nm thick layer of oxide. The sample is then transferred to a standard TEM grid (Quantumfoil) (Fig. 1b) using a wedging transfer technique [20] with some modifications. A thin layer of hydrophobic polymer cellulose acetate butyrate (30 mg/mL in ethyl acetate) is spun on top of the silicon wafer with the graphene sample at 1000 rpm for 30 seconds. The polymer film is then wedging floated on water together with the graphene sample. The hydrophobic film is aligned under an optical microscope and deposited on the TEM grid before being washed away with acetone, leaving the graphene membrane suspended on the TEM grid.

**Imaging the graphene membrane with TEM.** The suspended graphene sample is imaged with Libra 200MC TEM from Carl Zeiss, a monochromatic, aberration-corrected TEM equipped with a field emission gun (80-200 kV) and an in-column energy filter. The aberration correction is applied with the CETCOR software interface (CEOS GmbH, Heidelberg, Germany) up to 3rd order. The spherical aberration is set at 5$\mu$m and a defocus of 5 nm (Scherzer defocus) is used. The monochromator takes effect with a 3.5 $\mu$m slit and the images are recorded by a 4000 $\times$ 4000 CCD camera (Gatan, Ultrascan4000, USA) at a nominal magnification of $10^6$. All image data reported in this paper were based on the same aberration correction parameters unless otherwise specified.

**First-principles calculations and TEM image simulation.** The total potentials of the FLG system and the carbon atom are calculated using the density functional theory (DFT) method with normconserving pseudopotentials [27] implemented in the `SIESTA` code [28]. The geometries of the FLG system were optimized using the conjugate gradient algorithm and a 0.04 eV/Å maximum force convergence criterion. The atomic potential of carbon is also calculated with the all-electron code `ATOM`, for the core correction term. In all cases, the generalized gradient approximation (GGA) exchange-correlation density functional PBE [29] was employed together with a double-$\zeta$ plus polarization basis set, and a mesh cutoff of 200 Ry. The total potential of the FLG system, after core-potential correction, is projected according to given tilt directions. TEM simulations are carried out based on the projected potential, and the calculations of electron waves and TEM images follow the procedures described for a thin specimen as in Chapter 3 of ref. 20.

**Image matching and topography reconstruction.** Image matching is implemented by calculating the cross-correlation of the experimental TEM images and the simulated images. A normalized cross-correlation functional [18] $C$ is computed in the search for the best match:

$$C(f_{exp}, f_{sim}) = \frac{\sum_{xy}(f_{exp}(x,y) - \overline{f}_{exp})(f_{sim}(x,y) - \overline{f}_{sim})}{\sqrt{\sum_{xy}(f_{exp}(x,y) - \overline{f}_{exp})^2 \sum_{xy}(f_{sim}(x,y) - \overline{f}_{sim})^2}} \quad (1)$$

where $f(x,y)$ is the local pixel intensity and $\overline{f}$ is the global intensity average. Each local contrast pattern from the TEM experiment is compared to all the simulated images based on the array of tilt angles. The

best matches are founded and the corresponding local inclinations yield the overall gradient field. Reconstruction of the topology from the gradient field is based on a nonlocal Fourier transform algorithm [25]. The reconstruction is coded as a self-consistent process where the input gradient field is compared to the gradient field computed for the reconstructed surface. The difference contributes with a weight to the fine tuning of the initial tilt angle matching.


[1] Geim, A. K. & Novoselov, K. S. The rise of graphene. *Nat. Mater.* **6**, 183-191, (2007).

[2] Novoselov, K. S.*et al.* Electric field effect in atomically thin carbon films. *Science* **306**, 666-669, (2004).

[3] Meyer, J. C. *et al.* The structure of suspended graphene sheets. *Nature* **446**, 60-63, (2007).

[4] Lee, C., Wei, X. D., Kysar, J. W. & Hone, J. Measurement of the elastic properties and intrinsic strength of monolayer graphene. *Science* **321**, 385-388, (2008).

[5] Nelson, D. R. & Peliti, L. Fluctuations in Membranes with Crystalline and Hexatic Order. *J Phys-Paris* **48**, 1085-1092, (1987).

[6] Fasolino, A., Los, J. H. & Katsnelson, M. I. Intrinsic ripples in graphene. *Nat. Mater.* **6**, 858-861, (2007).

[7] Meyer, J. C. *et al.* On the roughness of single- and bi-layer graphene membranes. *Solid State Commun.* **143**, 101-109, (2007).

[8] Striemer, C. C., Gaborski, T. R., McGrath, J. L. & Fauchet, P. M. Charge- and size-based separation of macromolecules using ultrathin silicon membranes. *Nature* **445**, 749-753, (2007).

[9] Mermin, N. D. Crystalline Order in Two Dimensions. *Physical Review* **176**, 250-254, (1968).

[10] Nelson, D. R., Piran, T. & Weinberg, S. Statistical mechanics of membranes and surfaces. 2nd edn, (World Scientific Pub., 2004).

[11] de Juan, F., Cortijo, A. & Vozmediano, M. A. H. Charge inhomogeneities due to smooth ripples in graphene sheets. *Phys. Rev. B* **76**, (2007).

[12] Herbut, I. F., Juricic, V. & Vafek, O. Coulomb interaction, ripples, and the minimal conductivity of graphene. *Phys. Rev. Lett.* **100**, (2008).

[13] Guinea, F., Horovitz, B. & Le Doussal, P. Gauge field induced by ripples in graphene. *Phys. Rev. B* **77**, (2008).

[14] Guinea, F., Horovitz, B. & Le Doussal, P. Gauge fields, ripples and wrinkles in graphene layers. *Solid State Commun.* **149**, 1140-1143, (2009).

[15] Miranda, R. & de Parga, A. L. V. Graphene Surfing ripples towards new devices. *Nat. Nanotechnol.* **4**, 549-550, (2009).

[16] Guinea, F., Katsnelson, M. I. & Geim, A. K. Energy gaps and a zero-field quantum Hall effect in graphene by strain engineering. *Nat. Phys.* **6**, 30-33, (2010).

[17] Bangert, U., Gass, M. H., Bleloch, A. L., Nair, R. R. & Geim, A. K. Manifestation of ripples in free-standing graphene in lattice images obtained in an aberration-corrected scanning transmission electron microscope. *Phys Status Solidi A* **206**, 1117-1122 (2009).

[18] Kirkland, E. J. Advanced computing in electron microscopy. (Springer, 2010).

[19] Meyer, J. C. *et al.* Experimental analysis of charge redistribution due to chemical bonding by high-resolution transmission electron microscopy. *Nat. Mater.* **10**, 209-215, (2011).

[20] Schneider, G. F., Calado, V. E., Zandbergen, H., Vandersypen, L. M. K.& Dekker, C. Wedging Transfer of Nanostructures. *Nano Lett.* **10**, 1912-1916, (2010).

[21] Ferrari, A. C. *et al.* Raman spectrum of graphene and graphene layers. *Phys. Rev. Lett.* **97**, 4, (2006).

[22] Bell, D. C., Russo, C. J. & Benner, G. Sub-Angstrom Low-Voltage Performance of a Monochromated, Aberration-Corrected Transmission Electron Microscope. *Microsc Microanal* **16**, 386-392, (2010).

[23] Singh, M. K.*et al.* Atomic-scale observation of rotational misorientation in suspended few-layer graphene sheets. *Nanoscale* **2**, 700-708, (2010).

[24] Mao, Y. D., Wang, W. L., Wei, D. G., Kaxiras, E. & Sodroski, J. G. Graphene Structures at an Extreme Degree of Buckling. *ACS Nano* **5**, 1395-1400, (2011).

[25] Wei, T. G. & Klette, R. Depth recovery from noisy gradient vector fields using regularization. *Lect Notes Comput Sc* **2756**, 116-123, (2003).

[26] Novoselov, K. S.*et al.* Two-dimensional atomic crystals. *Proc. Natl. Acad. Sci. U. S. A.* **102**, 10451-10453, (2005).

[27] Kresse, G. & Joubert, D. From ultrasoft pseudopotentials to the projector augmented-wave method. *Phys. Rev. B* **59**, 1758-1775, (1999).

[28] Soler, J. M.*et al.* The SIESTA method for ab initio order-N materials simulation. *J. Phys.-Condes. Matter* **14**, 2745-2779, (2002).

[29] Perdew, J. P., Burke, K. & Ernzerhof, M. Generalized gradient approximation made simple. *Phys. Rev. Lett.* **77**, 3865-3868, (1996).

**FIG.1: Sample preparation and direct TEM imaging of graphene membrane.** All images are unfiltered. The scale bar in **b**, **c**, and **d** are 2 nm, 0.5 nm, and 2nm respectively. **a,** Partially suspended graphene flake across 1.2 $\mu$m holes of a standard TEM grid. Sample is examined with Raman spectroscopy and signatures for both SLG (red) and FLG (green) areas are identified, distinguished by the width and intensity ratio of the G and 2D peaks [21]. **b,** Fold at the edge of graphene membrane shows that the FLG area has 11 layers. **c,** TEM image of the FLG region. Fast Fourier transform of the image shown in the inset demonstrate a resolution better than 0.79 Å. **d,** TEM images of the FLG sample with a range of 50 nm $\times$ 50 nm area. A $4 \times 3$ array of samples is enlarged and shown on top of the original image. The size of each inset image is 8 Å$\times$ 8 Å. **e,** A selected area in the original TEM image is plotted with color, showing the gradually varying TEM contrast pattern.

**FIG.2: Calculations of total potential based on first-principles and its effect on TEM contrast.** **a.** Construction of the DFT total potential and comparison to the potential based on IAM. Distance $r$ is measured from one nucleus, and the plot is over a range corresponding to one bond length shown in the inset. The black dashed curve $V_{atom}$ is the total potential of a single carbon atom obtained from all-electron calculations. The cyan curve $V_{cc}$ is the core-correction potential, with a cutoff at a core radius of $r_0 = 0.6$ Å. $V_{IAM}$ (blue solid line), and $V_{ps}$ (red dashed line) are the total potentials for graphene calculated based on IAM, and pseudopotential DFT, respectively. The core-corrected total potential $V_{ps-cc}$ (red solid line) based on pseudopotential DFT calculations retains the correct potential in the bonding region while it recovers the correct potential in the core region. The inset shows the potential difference between $V_{ps-cc}$ and $V_{IAM}$, where blue is small and dark red is large and the total range is 50 V. **b.** Effects of DFT vs. IAM potentials on TEM imaging. The upper left is the simulated TEM image of a FLG (11 layers) with a local tilt of $\theta_x = 4.5^o$ and $\theta_y = 2.5^o$. The upper right image is the contrast difference between normalized TEM images based on DFT and IAM potentials. Both scale bars are 1 Å. The profiles measured along the the red dashed lines are shown in the lower right figure for three parameter combinations of spherical aberration and defocus values, namely, ($C_s1 = 6\mu$m, $\Delta Z = -3$nm), ($C_s2 = 4\mu$m, $\Delta Z = -2$nm), and ($C_s3 = 2\mu$m, $\Delta Z = -1$nm). The corresponding contrast transfer functions are shown in the lower left plot. The general trend is that as the spherical aberration decreases the error of using IAM over DFT potential becomes larger.

**FIG.3: Image matching from experiment to simulations.** **a** Identified best matches for various patterns. On the left are the unfiltered TEM images, and on the right the simulated images, with a plot of the vectors showing the direction and the amplitude of the corresponding tilt of the surface normal. **b,** The vectors in the x-y plane are the projection of the tilted normal **n**. The amplitude of the vectors are scaled to the red dashed circle that marks the tilt angle of the normal $\theta = 7^o$. The tangent of the angle $\theta_x$ and $\theta_y$ are the gradient of the surface. **c,** The matching index landscape of one of the pairs (lower right one). The contour map shows the value of the normalized cross-correlation function for various combinations of the gradient in the x and y directions. The two maxima (best matches) are indicated by arrows.

**FIG.4: Reconstruction of membrane topography based on the matched gradient field. a,** Topography of the reconstructed membrane surface and the corresponding contour plots. Scale in vertical direction is amplified for visualization. For the shown size of $50 \times 50$ nm area, the out-of-plane displacement is 0.5 nm with a standard deviation of 0.13 nm. The typical width of the ripple is 30 nm, as is indicated by the arrow in the contour plot. **b,** Comparison of the gradient $(p, q)$ from TEM matching and that of the reconstructed surface $(p', q')$. The diagonal profiles shown in the insets are plotted.

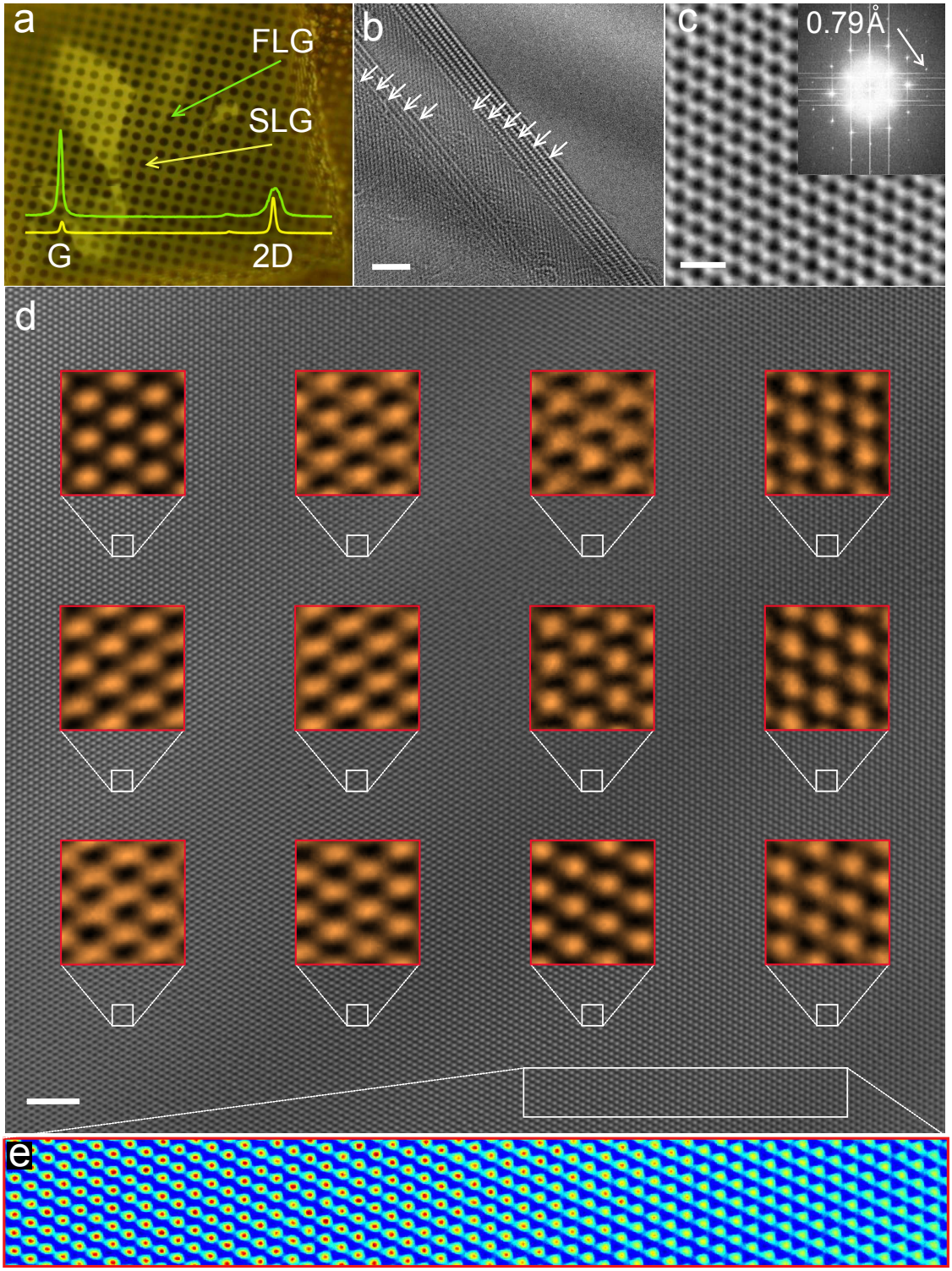


FIG. 1: **Sample preparation and direct TEM imaging of graphene membrane.**

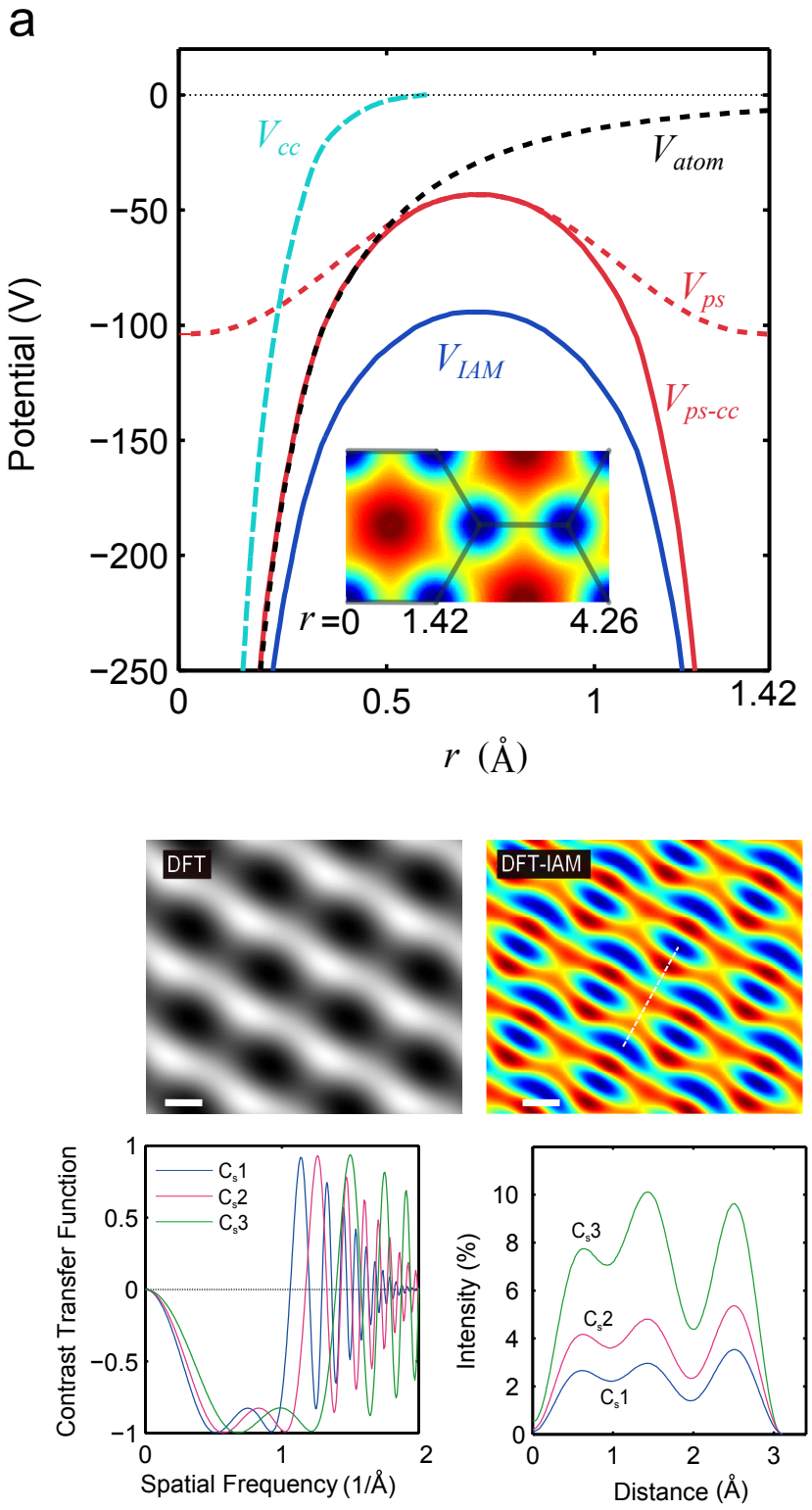


FIG. 2: **Calculations of total potential based on first-principles.**

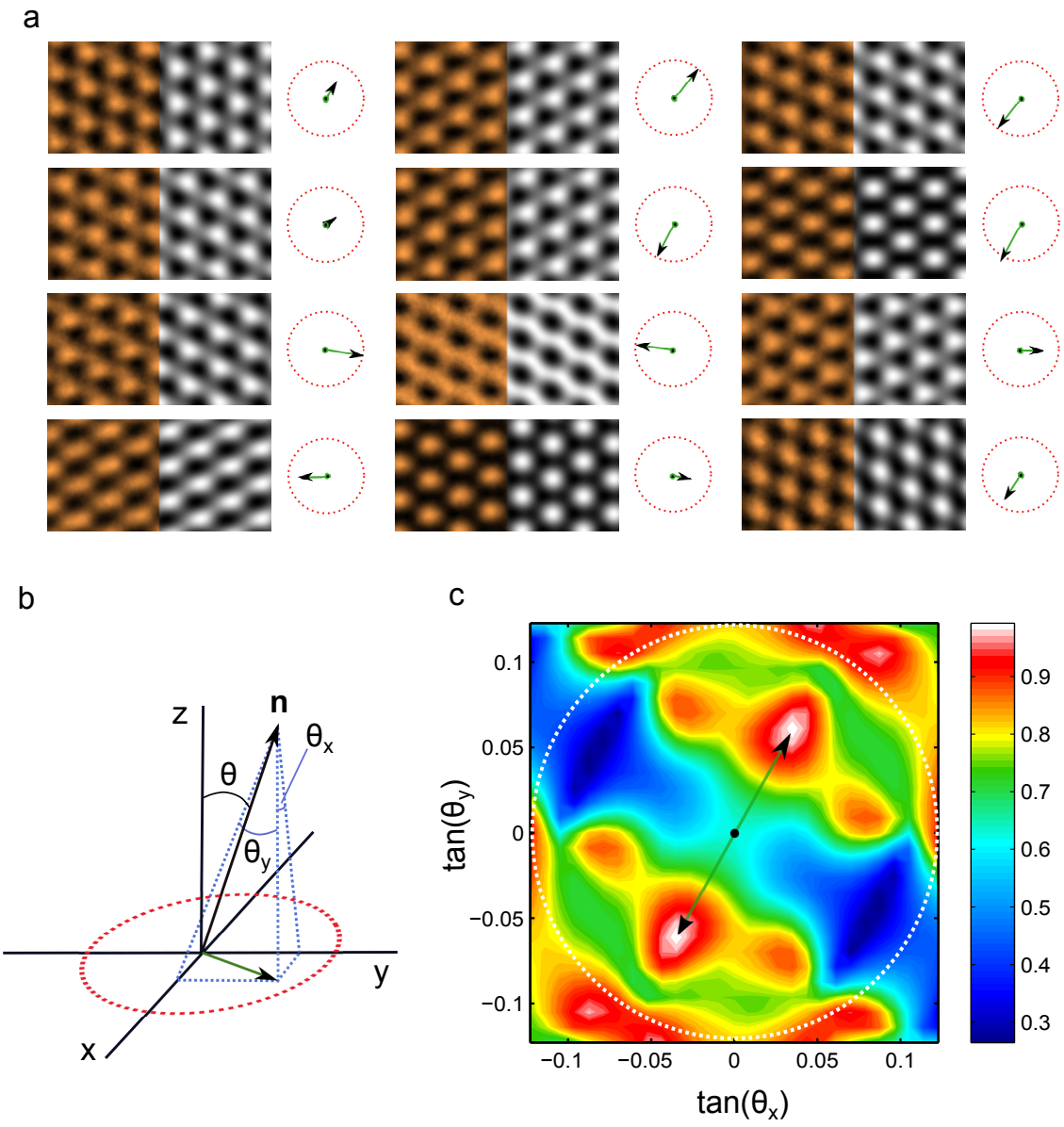


FIG. 3: **Image matching from experiment to simulations.**

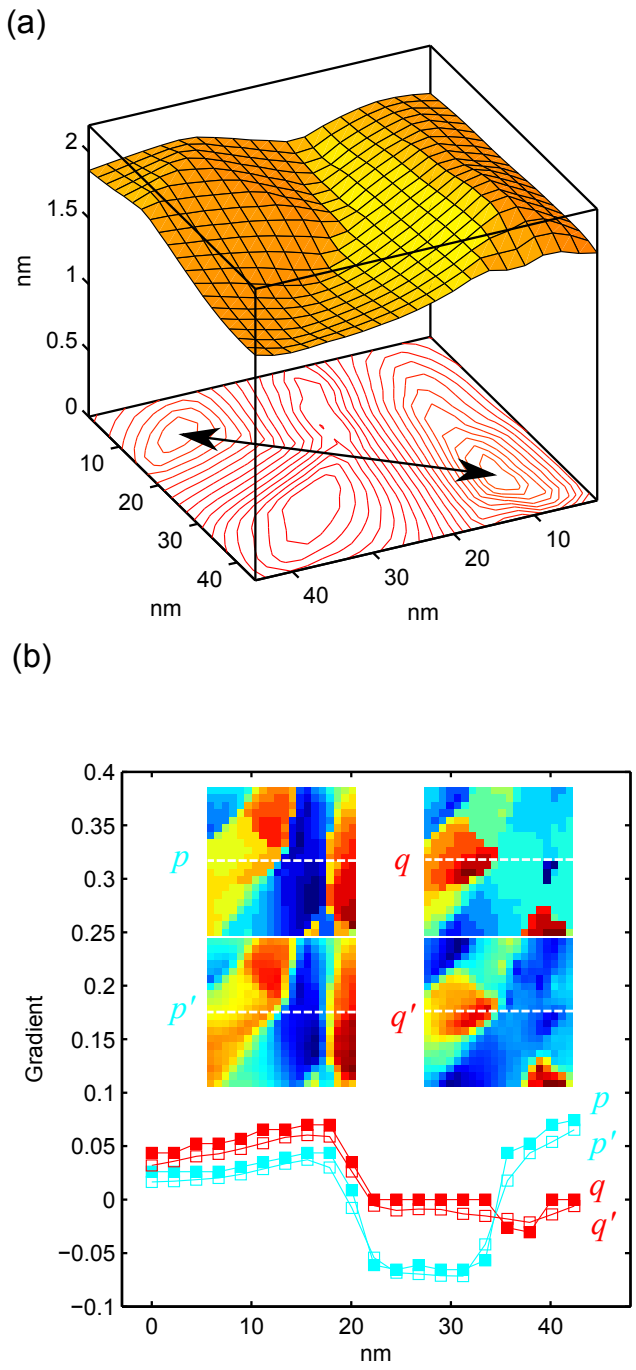


FIG. 4: **Reconstruction of membrane topography based on the matched gradient field.**